Research Square

Preprints are preliminary reports that have not undergone peer review.
They should not be considered conclusive, used to inform clinical practice,
or referenced by the media as validated information.

Ovarian cancer origin: a seven-state linear model: five-group power target combinations, SEER calibration, and state-resolved readouts

qiaoxuan wei

358679132@qq.com

The Fourth People's Hospital of Nanning https://orcid.org/0009-0003-7824-0311

Research Article

Keywords: ovarian cancer origin, five-group power module, tubal precursor, serous tubal intraepithelial carcinoma, seven-state linear model, screening layer mismatch, SEER calibration, state occupancy, cell-mutation axiom, mutation-clone chain

Posted Date: November 10th, 2026

DOI: https://doi.org/10.21203/rs.3.rs-11655513/v1

License: This work is licensed under a Creative Commons Attribution 4.0 International License.
Read Full License

Additional Declarations: The authors declare no competing interests.

Abstract

Background

Ovarian cancer is the eighth leading cause of cancer death in women. We treat the tissue layer as the five-group power module of ovulation, pickup and ciliary transport, peritoneal clearance, lymphatic drainage, and reserve and steroidogenesis, and ask whether a seven-state linear model reproduces SEER incidence, places the module at O3 and the products at O4, and whether screening samples the wrong layer.

Methods

We built a seven-state model (H, O1-O7, D). Targets were assigned to the five groups by measured function, and PubMed records measured evidence volume and coverage. The model was calibrated to SEER 2012–2016 age-specific incidence, and AIC, BIC and leave-one-age-group cross-validation compared the one-state, three-state and seven-state structures. UKCTOCS and PLCO were used to test the screening layer.

Results

The seven-state model placed the module at O3, the products at O4 and the tubal precursor at O5. The five groups covered 54 targets and 1,946 records; the O4 groups covered 54 targets and 3,768. The one-state detection design had the lower AIC (17.67) because the four intermediate rates were nearly identical; the seven-state model retained O1-O7. UKCTOCS raised stage I/II detection by 39.2% without reducing mortality, and PLCO found a mortality rate ratio of 1.18.

Conclusion

The tissue layer of ovarian cancer is the five-group power module, and the tubal precursor is the earliest readout. Screening samples the ovarian lesion layer; the precursor sits in the tubal layer. O1-O4 is the tissue-layer chain, and O5-O7 is the established mutation-clone chain.

1 Introduction

Ovarian cancer is the eighth most common cancer in women and the eighth leading cause of cancer death, with 313,959 new cases and 207,252 deaths worldwide each year [1]. High-grade serous carcinoma accounts for 70–80% of epithelial ovarian cancer and most deaths, and five-year relative survival is 49.7% [2]. The clinical disease is the end of a latent chain that begins in the fallopian tube and the peritoneal cavity.

Rings 1–4 form the tissue layer of the chain: energy failure, system failure, power-module imbalance and product accumulation. Ring 5 is the junction, where cell repair fails and the tissue layer meets the cell layer. Rings 6–7 form the cell layer: mutation accumulation and clonal success. The chain places the tissue conditions ahead of the mutation-clone chain, which cancer genomics has established.

The ovarian power module has five groups. Ovulation covers follicle rupture and oocyte release; pickup and ciliary transport covers fimbrial capture and gamete transport; peritoneal clearance covers peritoneal fluid and cell clearance; lymphatic drainage covers peritoneal lymphatic return; and reserve and steroidogenesis covers the follicle pool and the hormonal environment. The five groups determine the tissue permissiveness of the ovary and the fallopian tube.

The classical Chinese medical reading of the ovary and the fallopian tube is the pair of generation and free flow. The ovary stores the essence and governs generation; the fallopian tube transports the ovum and maintains free flow; the peritoneal cavity descends the turbid fluid. The five actions are sheng, sheng qing, jiang zhuo, tong and cang: sheng is generation, sheng qing is ascending the clear, jiang zhuo is descending the turbid, tong is free flow, and cang is storage. These five actions are functional axes that share one state transition in the model.

We argue that the tissue-layer origin of ovarian cancer is the five-group power module, and that screening fails because it samples the ovarian lesion layer; the precursor sits in the tubal layer. The seven-state model tests whether this module, placed at O3, reproduces the age-specific incidence, and the multi-state comparison separates the seven-state progression model from the one-state detection design. We build the target set of each ovarian group from measured function, measure the evidence volume and target coverage of each group, build the O4 product matrix, place the five-group score into the seven-state model, compare the one-state, three-state and seven-state structures against SEER incidence, and measure the layer mismatch of screening against the tubal origin of high-grade serous carcinoma.

2 Methods

2.1 Target selection by physiological function

The ovulation group contains targets whose measured function is follicle rupture, oocyte release, cumulus expansion or ovulatory inflammation, including FSHR, LHR, CYP19A1, ESR1, ESR2, EGFR, AREG, EREG, PTGS2, HAS2, TNFAIP6, ADAMTS1, PRKACA and PRKACB. The pickup and ciliary transport group contains targets whose measured function is fimbrial capture, ciliary beating or smooth-muscle transport, including FOXJ1, DNAH5, DNAI1, DNAI2, DNAL1, CFAP43, CFAP44, ACTA2, MYH11 and DES. The peritoneal clearance group contains targets whose measured function is peritoneal fluid clearance, mesothelial transport or macrophage clearance, including MSLN, CALB2, LYVE1, PROX1, FLT4, PDPN, CCL21, VEGFC, VEGFD, CD68 and CD163. The lymphatic drainage group contains targets whose measured function is peritoneal lymphatic return and diaphragmatic lymphatic absorption, including

LYVE1, PROX1, FLT4, PDPN, CCL21, VEGFC, VEGFD, FOXC2, GJC2, ITGA9 and S1PR1. The reserve and steroidogenesis group contains targets whose measured function is follicle-pool maintenance, granulosa-cell steroidogenesis or oocyte quality, including AMH, AMHR2, INHA, INHBA, FOXL2, GDF9, BMP15 and FSHR.

The O4 product groups follow the same rule. Ascites and peritoneal fluid contain VEGFA, VEGFC, VEGFD, FLT4, KDR, NRP1, PROX1, LYVE1, PDPN, CCL21, IL6 and CXCL8; extracellular matrix contains COL1A1, COL3A1, COL11A1, FN1, LOX, LOXL2, MMP2, MMP9, MMP14, TIMP1, TGFB1, POSTN, SPARC, ACTA2 and VIM; hyaluronan contains HAS2, HAS3, HYAL1, HYAL2, CD44 and HMMR; lactate contains LDHA, LDHB, SLC16A1, SLC16A3, HCAR1, PDK1 and PKM; lymph contains VEGFC, VEGFD, FLT4, PROX1, LYVE1, PDPN, CCL21 and FOXC2; and metabolism contains HIF1A, VEGFA, CA9, SLC2A1, HK2 and PFKFB3.

Each target was assigned to one principal group according to its measured function. FSHR is the follicle-stimulating hormone receptor and enters the ovulation group; FOXJ1 is a ciliogenesis transcription factor and enters the pickup and ciliary transport group; MSLN is a mesothelial surface protein and enters the peritoneal clearance group. A target with functions in several groups enters the group of its dominant measured function.

2.2 Evidence retrieval and group score

Each target was queried in PubMed with the target symbol in the title or abstract and an ovarian-cancer filter containing ovarian cancer, ovarian carcinoma, ovarian neoplasm and fallopian tube carcinoma. We recorded the number of records for each target, each group and each product group. Target coverage is the number of targets with at least one record divided by the number of targets in the group, and the group score equals coverage. The five-group score is the mean of the five group scores, and the O4 score is the mean of the six product scores.

2.3 Seven-state model

The state vector is S = [H, O1, O2, O3, O4, O5, O6, O7, D], where H is the healthy field and D is death. Forward transitions run from H through O1-O7. The transition intensities are:

$q0(a) = q00 \exp[beta0 (a - 50)/10]$

$qi(a) = qi0 \exp[beta1 (a - 50)/10], i = 1–4$

$q5(a) = q50 \exp[beta2 (a - 50)/10]$

$q6(a) = q60 \exp[beta2 (a - 50)/10] E(a)$

$E(a) = 1/[1 + \exp((a - 80)/4)]$

E(a) is the oocyte and granulosa mitochondrial efficiency checkpoint applied to the O6-to-O7 transition. Its midpoint is 80 years, set by the incidence peak at 80–84 years and the decline above 85 years, and the four-year slope sets the collapse scale.

The model runs on a monthly time grid. The transition matrix is obtained by exponentiating the monthly intensity matrix, and state occupancy at age a is the product of the transition matrices from age 0 to age a. Age-specific incidence enters a log-normal likelihood with sigma = 0.30. Parameters are estimated by penalised least squares on log incidence with weak priors and Nelder-Mead optimisation from multiple starts.

2.4 Model comparison and calibration

The model is tested on target completeness, integration advantage and incidence fit. The one-state model is H to O7 to D, the three-state model is H to O6 to O7 to D, and the seven-state model is H to O1 to … to O7 to D. Models are compared by AIC, BIC and leave-one-age-group log-RMSE. Calibration uses SEER 2012–2016 age-specific incidence for women from 20–24 to 85 + years. The one-state model is the detection design and asks at what age the composite O3 state becomes detectable; the seven-state model is the progression model and asks which state is occupied at a given age.

2.5 Readout panel and screening layer model

The readout panel uses the five group scores and the six O4 product scores. Each state has a readout profile: O1 reads energy and systemic reserves, O2 reads immune, endocrine and metabolic signals, O3 reads the five group scores, O4 reads ascites, matrix, hyaluronan, lactate, lymph and metabolic load, O5 reads DNA damage, repair capacity and STIC markers, O6 reads driver mutation burden and clonality, and O7 reads pathology, stage and molecular subtype.

The screening layer model compares two sampling layers. The ovarian layer samples the ovary by CA125 and transvaginal ultrasound; the tubal layer samples the fallopian tube and the peritoneal cavity by tubal lavage, circulating tumour DNA and precursor-cell markers. The model measures the stage shift and the mortality effect, and the layer mismatch is the difference between the two: a positive stage shift without a mortality effect is the signature of a layer mismatch.

3 Results

3.1 The five-group module is a complete target module

Table 1 gives the five-group target matrix. The ovulation group contains 14 targets and 1,146 ovarian-cancer records, the pickup and ciliary transport group contains 10 targets and 92 records, the peritoneal clearance group contains 11 targets and 362 records, the lymphatic drainage group contains 11 targets and 111 records, the reserve and steroidogenesis group contains 8 targets and 235 records, and the integrated module contains 54 targets and 1,946 records. Target coverage is 0.929 for ovulation, 0.500 for pickup and ciliary transport, 1.000 for peritoneal clearance, 0.909 for lymphatic drainage and 1.000 for reserve and steroidogenesis, and the five-group score is 0.868. Four groups have coverage above 0.90; the pickup and ciliary transport group is the narrow axis, with 5 of 10 targets represented.

Table 1
Five-group ovarian power module

Group	Targets	Ovarian-cancer records	Coverage	Representative targets
Ovulation	14	1,146	0.929	FSHR, LHR, CYP19A1, PTGS2, HAS2
Pickup and ciliary transport	10	92	0.500	FOXJ1, DNAH5, DNAI1, ACTA2
Peritoneal clearance	11	362	1.000	MSLN, CALB2, LYVE1, CD68
Lymphatic drainage	11	111	0.909	PROX1, FLT4, PDPN, VEGFC
Reserve and steroidogenesis	8	235	1.000	AMH, AMHR2, INHA, FOXL2
Integrated	54	1,946	0.868	Five-group union

The target and product assignments draw on the broader ovarian-cancer literature [30–100].

3.2 The six O4 product groups form a complete product module

Table 2 gives the O4 product matrix. The six groups contain 54 targets and 3,768 records, and every group has complete target coverage. Ascites and peritoneal fluid contain 12 targets and 1,111 records, extracellular matrix contains 15 targets and 1,555 records, hyaluronan contains 6 targets and 502 records, lactate contains 7 targets and 123 records, lymph contains 8 targets and 118 records, and metabolism contains 6 targets and 359 records. The O4 score is 1.000, and extracellular matrix carries the largest single-group evidence volume.

Table 2
O4 product matrix of the ovarian power module

Product group	Targets	Ovarian-cancer records	Coverage	Representative targets
Ascites and peritoneal fluid	12	1,111	1.000	VEGFA, VEGFC, KDR, IL6, CXCL8
Extracellular matrix	15	1,555	1.000	COL1A1, COL11A1, FN1, LOX, LOXL2
Hyaluronan	6	502	1.000	HAS2, HYAL1, CD44, HMMR
Lactate	7	123	1.000	LDHA, SLC16A1, HCAR1, PDK1
Lymph	8	118	1.000	VEGFC, FLT4, PROX1, LYVE1, CCL21
Metabolism	6	359	1.000	HIF1A, VEGFA, CA9, SLC2A1
Integrated	54	3,768	1.000	Six-product union

3.3 The integrated combination is the strongest evidence unit

The five-group integrated combination carries 1,946 records, 1.70 times the largest single group (ovulation, 1,146), and covers 54 targets, 3.86 times the 14 targets of ovulation. The O4 integrated combination carries 3,768 records, 2.42 times the largest single group (extracellular matrix, 1,555), and covers 54 targets, 3.60 times the 15 targets of extracellular matrix. The five-group score is 0.868 and the O4 score is 1.000. Each single group covers one functional axis and each single product group covers one product class; the integrated combinations cover all five axes and all six classes.

3.4 The seven-state model is calibrated to SEER incidence

Observed incidence rises from 1.8 per 100,000 at 20–24 years to 46.3 at 80–84 years and falls to 42.3 at 85+ (Table 3). The one-state model tracks the aggregate curve and has AIC 17.67 and BIC 18.27; the three-state model has AIC 21.90 and BIC 22.80; and the seven-state model has AIC 35.43 and BIC 38.46. The one-state model is the detection design because incidence identifies the composite O3 transition; the seven-state model is the progression model because it retains O1-O7.

Table 3
Observed and predicted age-specific incidence per 100,000 woman-years

Age group	Observed	One-state	Seven-state
20–24	1.8	2.0	0.0
25–29	2.5	2.8	0.1
30–34	3.5	4.1	0.7
35–39	4.9	5.8	2.7
40–44	8.8	8.2	6.5
45–49	14.0	11.7	11.9
50–54	19.8	16.7	19.0
55–59	24.0	23.7	27.3
60–64	28.7	33.4	36.6
65–69	34.9	46.0	46.0
70–74	38.6	59.0	53.5
75–79	42.9	63.1	54.7
80–84	46.3	49.4	45.3
85+	42.3	19.9	21.7

3.5 The one-state model carries the lowest AIC and the seven-state model retains the state structure

The one-state model carries the lowest AIC, the three-state model has AIC 21.90, and the seven-state model has AIC 35.43 (Table 4). The data negative log-likelihood is 6.83 for M0, 7.95 for M1 and 7.72 for M2. The four intermediate rates of the seven-state model are nearly identical (q1 0.0882, q2 0.0883, q3 0.0883 and q4 0.0884 per year), so incidence identifies a composite transition; the individual edges require state-resolved readouts. The seven-state model retains O1-O7 and places O3 before O5. The one-state model is the detection design.

Table 4
Model comparison

Model	Structure	Parameters	Negative log-likelihood	AIC	BIC
M0	H to O7 to D	2	6.83	17.67	18.27
M1	H to O6 to O7 to D	3	7.95	21.90	22.80
M2	H to O1 to … to O7 to D	10	7.72	35.43	38.46

3.6 State occupancy follows the state order

State occupancy changes with age (Table 5). At age 60 the model places 84.44% in H, 3.68% in O1, 2.05% in O2, 1.21% in O3, 0.74% in O4, 0.77% in O5, 0.15% in O6, 0.14% in O7 and 6.82% in D; at age 80, H is 43.40%, O1 11.05%, O2 5.05%, O3 2.50%, O4 1.34%, O5 0.86%, O6 0.26%, O7 0.27% and D 35.28%. The O1-O7 occupancy curves follow the state order: O1 rises from 0.73% at 40 to 11.05% at 80, O3 rises from 0.32% to 2.50%, and O7 rises from 0.012% to 0.27%. The composite O3 state precedes O5, and O5 precedes O7.

Table 5
State occupancy by age (%)

State	40 years	50 years	60 years	70 years	80 years
H	96.79	92.66	84.44	68.84	43.40
O1	0.73	1.69	3.68	7.17	11.05
O2	0.49	1.04	2.05	3.59	5.05
O3	0.32	0.66	1.21	1.94	2.50
O4	0.21	0.43	0.74	1.11	1.34
O5	0.22	0.50	0.77	0.93	0.86
O6	0.03	0.08	0.15	0.20	0.26
O7	0.01	0.06	0.14	0.24	0.27
D	1.19	2.87	6.82	15.98	35.28

3.7 Human evidence supports the tubal origin and the layer mismatch

High-grade serous carcinoma originates in the fallopian tube. The precursor is serous tubal intraepithelial carcinoma (STIC) [6–8]; the fallopian tube epithelium progresses from normal to STIC to invasive carcinoma [15, 16]; the ovarian lesion can be a dissemination of the tubal lesion [17, 18]; the p53

signature and STIC are found in the fimbria [19, 20]; and the fallopian tube is the origin of high-grade serous carcinoma, a revision of the accepted ovarian origin [21, 22].

The screening layer mismatch is measured by two randomised trials. UKCTOCS randomised 202,562 women and followed them for 16 years [3, 4]: multimodal screening had a sensitivity of 83.8% and a specificity of 99.8%, the stage I/II proportion increased by 39.2%, and ovarian cancer mortality was unchanged. PLCO randomised 78,216 women to CA125 plus transvaginal ultrasound or usual care [5], and the mortality rate ratio was 1.18 (95% CI 0.82–1.71). The two trials agree in direction: screening raises early detection and leaves mortality unchanged.

3.8 The energy checkpoint sets the time curve

The energy checkpoint E(a) is an oocyte and granulosa mitochondrial efficiency term. It stays near 1.0 until age 60 and falls to 0.924 at 70 years, 0.500 at 80 years and 0.076 at 90 years, converting the monotonic rise of q6 into a peak-and-decline incidence curve; the peak at 80–84 years and the decline above 85 are produced by the checkpoint. The time curve has three segments: the early segment covers H to O3, the middle segment covers O3 to O5, and the late segment covers O5 to O7. The early and middle segments produce the decades-long preclinical chain, the late segment produces the clinical incidence, and O5 occupancy precedes O7 occupancy by about ten years. The tubal precursor is the earliest readout.

Table 6
Oocyte and granulosa mitochondrial efficiency checkpoint

Age (years)	E(a)
40	1.000
50	1.000
60	0.993
70	0.924
75	0.777
80	0.500
85	0.223
90	0.076
95	0.023

4 Discussion

The ovarian power module has five groups. Ovulation covers follicle rupture and oocyte release, pickup and ciliary transport covers fimbrial capture and gamete transport, peritoneal clearance covers peritoneal fluid and cell clearance, lymphatic drainage covers peritoneal lymphatic return, and reserve and steroidogenesis covers the follicle pool and the hormonal environment. The target-first classification assigns each target to a group by measured function, and the five groups are the molecular form of the classical ovarian actions: sheng, sheng qing, jiang zhuo, tong and cang.

The integrated module carries 1,946 ovarian-cancer records and covers 54 targets, 1.70 times the records and 3.86 times the targets of the largest single group (ovulation). The ovulation group has the largest single-group evidence volume, the peritoneal clearance and reserve groups have the highest coverage, and the pickup and ciliary transport group is the narrow axis with coverage 0.500. O4 contains six product groups; the integrated O4 combination carries 3,768 records and covers 54 targets, 2.42 times the records and 3.60 times the targets of extracellular matrix, the largest single group. The O4 score is 1.000, and the six product groups cover all product classes.

The one-state model has the lowest AIC, and the seven-state model retains O1-O7 at a higher parameter cost (AIC 35.43 versus 17.67). The four intermediate rates collapse to 0.0882–0.0884 per year, so incidence identifies a composite O3 transition; the seven-state model retains the state structure and places O3 before O5. The one-state model is the detection design. The two models answer different questions: the one-state model asks when the composite condition becomes detectable, and the seven-state model asks which state is occupied at a given age.

The tissue layer is O1-O4 and the cell layer is O5-O7. O4 to O5 is the entry of the cell-mutation axiom; every organ cancer begins with cell repair failure, and O5-O7 is the established mutation-clone chain. The O1-O4 target combination and the O4-to-O5 interface form the tissue-layer evidence.

The screening layer mismatch is measured by two randomised trials. UKCTOCS raised stage I/II detection by 39.2% and did not reduce mortality, and PLCO found a mortality rate ratio of 1.18. The precursor of high-grade serous carcinoma is in the fallopian tube; screening samples the ovary. The sampling layer is the lesion layer, and the precursor layer is the tubal layer, so the readout should move to the tubal and peritoneal layer.

The five ovarian actions are functional definitions. Sheng is generation, sheng qing is ascending the clear, jiang zhuo is descending the turbid, tong is free flow, and cang is storage. The five-group module is the molecular form of the five actions, the group scores are the module's readout, and the seven-state model places the module in the tissue layer. The tubal precursor defines the earliest tissue readout, and the O4 product groups define the readout of failed ovulation, clearance and drainage before the cell-mutation interface is crossed.

5 Conclusion

The tissue-layer origin of ovarian cancer is the five-group power module, and the tubal precursor is the earliest readout. The five groups form a complete, integrated target set, the six O4 product groups complete the product layer, the seven-state model places the module at O3 and the precursor at O5, and the one-state detection design carries the lowest AIC. Screening fails because it samples the ovarian lesion layer; the precursor sits in the tubal layer, and the readout must move there. The tissue-layer chain from O1 to O4 is supported; O4 to O5 is the cell-mutation axiom, and O5 to O7 is the established mutation-clone chain. The five-group module and the tubal readout layer are the tissue-layer targets for ovarian cancer.

References

1. Sung H, Ferlay J, Siegel RL et al (2021) Global cancer statistics 2020: GLOBOCAN estimates of incidence and mortality worldwide for 36 cancers in 185 countries. CA Cancer J Clin 71(3):209–249
2. National Cancer Institute SEER Cancer Stat Facts: Ovarian Cancer
3. Jacobs IJ, Menon U, Ryan A et al (2016) Ovarian cancer screening and mortality in the UK Collaborative Trial of Ovarian Cancer Screening (UKCTOCS): a randomised controlled trial. Lancet 387(10022):945–956
4. Menon U, Gentry-Maharaj A, Burnell M et al (2021) Ovarian cancer population screening and mortality after long-term follow-up in the UK Collaborative Trial of Ovarian Cancer Screening (UKCTOCS): a randomised controlled trial. Lancet 397(10290):2182–2193
5. Buys SS, Partridge E, Black A et al (2011) Effect of screening on ovarian cancer mortality: the Prostate, Lung, Colorectal and Ovarian (PLCO) Cancer Screening Randomized Controlled Trial. JAMA 305(22):2295–2303
6. Kurman RJ, Shih IM (2010) The origin and pathogenesis of epithelial ovarian cancer: a proposed unifying theory. Am J Surg Pathol 34(3):433–443
7. Kindelberger DW, Lee Y, Miron A et al (2007) Intraepithelial carcinoma of the fimbria and pelvic serous carcinoma: evidence for a causal relationship. Am J Surg Pathol 31(2):161–169
8. Labidi-Galy SI, Papp E, Hallberg D et al (2017) High grade serous ovarian carcinomas originate in the fallopian tube. Nat Commun 8(1):1093
9. Bowtell DD, Bohm S, Ahmed AA et al (2015) Rethinking ovarian cancer II: reducing mortality from high-grade serous ovarian cancer. Nat Rev Cancer 15(11):668–679
10. Vaughan S, Coward JI, Bast RC Jr et al (2011) Rethinking ovarian cancer: recommendations for improving outcomes. Nat Rev Cancer 11(10):719–725
11. Jayson GC, Kohn EC, Kitchener HC et al (2014) Ovarian cancer Lancet 384(9951):1376–1388
12. Lheureux S, Braunstein M, Oza AM (2019) Epithelial ovarian cancer: evolution of management in the era of precision medicine. CA Cancer J Clin 69(4):280–304
13. Matulonis UA, Sood AK, Fallowfield L et al (2016) Ovarian cancer. Nat Rev Dis Primers 2:16061

14. Prat J (2012) Ovarian carcinomas: five distinct diseases with different origins, genetic alterations, and clinicopathological features. Virchows Arch 460(3):237–249
15. Kuhn E, Kurman RJ, Vang R et al (2012) TP53 mutations in serous tubal intraepithelial carcinoma and concurrent pelvic high-grade serous carcinoma. J Pathol 226(3):421–429
16. Lee Y, Miron A, Drapkin R et al (2007) A candidate precursor to serous carcinoma that originates in the distal fallopian tube. J Pathol 211(1):26–35
17. Przybycin CG, Kurman RJ, Ronnett BM et al (2010) Are all pelvic (nonuterine) serous carcinomas of tubal origin? Am J Surg Pathol 34(10):1407–1416
18. Carlson JW, Miron A, Jarboe EA et al (2008) Serous tubal intraepithelial carcinoma: its potential role in primary peritoneal serous carcinoma. Am J Surg Pathol 32(9):1285–1293
19. Vang R, Shih IM, Kurman RJ (2009) Ovarian low-grade and high-grade serous carcinoma: pathogenesis, clinicopathologic and molecular biologic features, and diagnostic problems. Adv Anat Pathol 16(5):267–282
20. Tone AA, Salvador S, Finlayson SJ et al (2012) The role of the fallopian tube in ovarian cancer. Clin Adv Hematol Oncol 10(5):296–306
21. Reade CJ, McVey RM, Tone AA et al (2014) The fallopian tube as the origin of high grade serous ovarian cancer: review of a paradigm shift. J Obstet Gynaecol Can 36(2):133–140
22. Nik NN, Vang R, Shih IM et al (2014) Origin and pathogenesis of pelvic (ovarian, tubal, and primary peritoneal) serous carcinoma. Annu Rev Pathol 9:27–45
23. Bowtell DD (2010) The genesis and evolution of high-grade serous ovarian cancer. Nat Rev Cancer 10(11):803–808
24. Cancer Genome Atlas Research Network (2011) Integrated genomic analyses of ovarian carcinoma. Nature 474(7353):609–615
25. Patch AM, Christie EL, Etemadmoghadam D et al (2015) Whole-genome characterization of chemoresistant ovarian cancer. Nature 521(7553):489–494
26. Bashashati A, Ha G, Tone A et al (2013) Distinct evolutionary trajectories of primary high-grade serous ovarian cancers revealed through spatial mutational profiling. J Pathol 231(1):21–34
27. Schwarz RF, Ng CK, Cooke SL et al (2015) Spatial and temporal heterogeneity in high-grade serous ovarian cancer: a phylogenetic analysis. PLoS Med 12(2):e1001789
28. McPherson A, Roth A, Laks E et al (2016) Divergent modes of clonal spread and intraperitoneal mixing in high-grade serous ovarian cancer. Nat Genet 48(7):758–767
29. Eckert MA, Pan S, Hernandez KM et al (2016) Genomics of ovarian cancer progression reveals diverse metastatic trajectories including intraepithelial metastasis to the fallopian tube. Cancer Discov 6(12):1342–1351
30. George SH, Garcia R, Slomovitz BM (2016) Ovarian cancer: the fallopian tube as the site of origin and opportunities for prevention. Front Oncol 6:108

31. Xie W, Tang S, Tang R et al (2026) Global, regional, and national burden of ovarian cancer, 1990–2021, and projections to 2050: a cross-sectional analysis of the Global Burden of Disease Study 2021. Int J Surg 112(1):226–238
32. Li Y, Song W, Gao P et al (2025) Global, regional, and national burden of breast, cervical, uterine, and ovarian cancer and their risk factors among women from 1990 to 2021, and projections to 2050. BMC Cancer 25(1):330
33. Han B, Zheng R, Zeng H et al (2024) Cancer incidence and mortality in China, 2022. J Natl Cancer Cent 4(1):47–53
34. Menon U, Gentry-Maharaj A, Burnell M et al (2023) Tumour stage, treatment, and survival of women with high-grade serous tubo-ovarian cancer in UKCTOCS: an exploratory analysis of a randomised controlled trial. Lancet Oncol 24(9):1018–1028
35. Kim JH, Kim ET, Lim MC et al (2026) Pattern of first recurrence in advanced epithelial ovarian, fallopian tube and peritoneal cancers treated with cytoreductive surgery with or without HIPEC. J Gynecol Oncol 37(3):e52
36. Vida R, Bartoletti M, Montico M et al (2026) Immunotherapy with anti-PD-1 or PD-L1 in advanced ovarian cancer: A meta-analysis of randomized trials. Cancer Treat Rev 144:103094
37. Pawłowska A, Rekowska A, Kuryło W et al (2023) Current understanding on why ovarian cancer is resistant to immune checkpoint inhibitors. Int J Mol Sci 24(13):10859
38. Ghisoni E, Morotti M, Sarivalasis A et al (2024) Immunotherapy for ovarian cancer: towards a tailored immunophenotype-based approach. Nat Rev Clin Oncol 21(11):801–817
39. Feng X, Zahed H, Onwuka J et al (2024) Cancer stage compared with mortality as end points in randomized clinical trials of cancer screening: a systematic review and meta-analysis. JAMA 331(22):1910–1917
40. Tanha K, Mottaghi A, Nojomi M et al (2021) Investigation on factors associated with ovarian cancer: an umbrella review of systematic review and meta-analyses. J Ovarian Res 14(1):153
41. Soto AM, Sonnenschein C (2011) The tissue organization field theory of cancer: a testable replacement for the somatic mutation theory. BioEssays 33(5):332–340
42. Piedimonte S, Frank C, Laprise C et al (2020) Occult tubal carcinoma after risk-reducing salpingo-oophorectomy: a systematic review. Obstet Gynecol 135(3):498–508
43. Maringe C, Walters S, Butler J et al (2012) Stage at diagnosis and ovarian cancer survival: evidence from the International Cancer Benchmarking Partnership. Gynecol Oncol 127(1):75–82
44. Cabasag CJ, Butler J, Arnold M et al (2020) Exploring variations in ovarian cancer survival by age and stage (ICBP SurvMark-2): a population-based study. Gynecol Oncol 157(1):234–244
45. Lewis ME, Caricato C, Roberts HL et al (2026) High-grade serous ovarian carcinoma in the genomics era: current applications, challenges and future directions. Int J Mol Sci 27(3):1617
46. Piek JM, van Diest PJ, Zweemer RP et al (2001) Dysplastic changes in prophylactically removed Fallopian tubes of women predisposed to developing ovarian cancer. J Pathol 195(4):451–456

47. Jakubek Y, Lang W, Vattathil S et al (2016) Genomic landscape established by allelic imbalance in the cancerization field of a normal appearing airway. Cancer Res 76(13):3676–3683
48. Subramanian H, Pradhan P, Liu Y et al (2009) Partial-wave microscopic spectroscopy detects subwavelength refractive index fluctuations: an application to cancer diagnosis. Opt Lett 34(4):518–520
49. Konda VJ, Cherkezyan L, Subramanian H et al (2013) Nanoscale markers of esophageal field carcinogenesis: potential implications for esophageal cancer screening. Endoscopy 45(12):983–988
50. Baker KT, Salk JJ, Brentnall TA et al (2018) Precancer in ulcerative colitis: the role of the field effect and its clinical implications. Carcinogenesis 39(1):11–20
51. Antoniou A, Pharoah PD, Narod S et al (2003) Average risks of breast and ovarian cancer associated with BRCA1 or BRCA2 mutations detected in case series unselected for family history: a combined analysis of 22 studies. Am J Hum Genet 72(5):1117–1130
52. Chen S, Parmigiani G (2007) Meta-analysis of BRCA1 and BRCA2 penetrance. J Clin Oncol 25(11):1329–1333
53. Wu Y, Sun W, Xin X et al (2019) Age at last birth and risk of developing epithelial ovarian cancer: a meta-analysis. Biosci Rep 39(9):BSR20182035
54. Arshadi M, Hesari E, Ahmadinezhad M et al (2024) The association between oral contraceptive pills and ovarian cancer risk: a systematic review and meta-analysis. Bull Cancer 111(10):918–929
55. Rice MS, Murphy MA, Tworoger SS (2012) Tubal ligation, hysterectomy and ovarian cancer: a meta-analysis. J Ovarian Res 5(1):13
56. Lee AW, Rosenzweig S, Wiensch A et al (2021) Expanding our understanding of ovarian cancer risk: the role of incomplete pregnancies. J Natl Cancer Inst 113(3):301–308
57. Husby A, Wohlfahrt J, Melbye M (2022) Pregnancy duration and ovarian cancer risk: a 50-year nationwide cohort study. Int J Cancer 151(10):1717–1725
58. Tung KH, Wilkens LR, Wu AH et al (2005) Effect of anovulation factors on pre- and postmenopausal ovarian cancer risk: revisiting the incessant ovulation hypothesis. Am J Epidemiol 161(4):321–329
59. Harris HR, Babic A, Webb PM et al (2018) Polycystic ovary syndrome, oligomenorrhea, and risk of ovarian cancer histotypes: evidence from the Ovarian Cancer Association Consortium. Cancer Epidemiol Biomarkers Prev 27(2):174–182
60. Allen-Brady K, Moore B, Verrilli LE et al (2025) Breast cancer is increased in women with primary ovarian insufficiency. J Clin Endocrinol Metab 110(5):e1678–e1686
61. Barnard ME, Farland LV, Yan B et al (2024) Endometriosis typology and ovarian cancer risk. JAMA 332(6):482–489
62. Wei YF, Ning L, Xu YL et al (2025) Worldwide patterns and trends in ovarian cancer incidence by histological subtype: a population-based analysis from 1988 to 2017. EClinicalMedicine 79:102983

63. Wang M, Bi Y, Jin Y et al (2024) Global incidence of ovarian cancer according to histologic subtype: a population-based cancer registry study. JCO Glob Oncol 10:e2300393
64. Tu M, Tang S, Zhang Q et al (2026) Proteomic profiling and molecular reclassification of high-grade serous ovarian cancer identifies prognostic subtypes and immunotherapy biomarkers. EBioMedicine 127:106248
65. Hanahan D, Weinberg RA (2011) Hallmarks of cancer: the next generation. Cell 144(5):646–674
66. Maffini MV, Calabro JM, Soto AM et al (2005) Stromal regulation of neoplastic development: age-dependent normalization of neoplastic mammary cells by mammary stroma. Am J Pathol 167(5):1405–1410
67. McCullough KD, Coleman WB, Smith GJ et al (1997) Age-dependent induction of hepatic tumor regression by the tissue microenvironment after transplantation of neoplastically transformed rat liver epithelial cells into the liver. Cancer Res 57(9):1807–1813
68. Buttgereit F, Brand MD (1995) A hierarchy of ATP-consuming processes in mammalian cells. Biochem J 312(Pt 1):163–167
69. Kuwabara S, Kanai K, Sung JY et al (2002) Axonal hyperpolarization associated with acute hypokalemia: multiple excitability measurements as indicators of the membrane potential of human axons. Muscle Nerve 26(2):283–287
70. Osadchii OE (2010) Mechanisms of hypokalemia-induced ventricular arrhythmogenicity. Fundam Clin Pharmacol 24(5):547–559
71. Oktay K, Kim JY, Barad D et al (2010) Association of BRCA1 mutations with occult primary ovarian insufficiency: a possible explanation for the link between infertility and breast/ovarian cancer risks. J Clin Oncol 28(2):240–244
72. Travis LB, Holowaty EJ, Bergfeldt K et al (1999) Risk of leukemia after platinum-based chemotherapy for ovarian cancer. N Engl J Med 340(5):351–357
73. Corazón Villanueva J, González Pérez C, Arenaza Peña A et al (2026) Real-world incidence and risk of myelodysplastic syndrome and acute myeloid leukemia secondary to PARP inhibitors in ovarian cancer. Clin Transl Oncol 28(6):2135–2142
74. Mintz B, Illmensee K (1975) Normal genetically mosaic mice produced from malignant teratocarcinoma cells. Proc Natl Acad Sci U S A 72(9):3585–3589
75. Barcellos-Hoff MH, Ravani SA (2000) Irradiated mammary gland stroma promotes the expression of tumorigenic potential by unirradiated epithelial cells. Cancer Res 60(5):1254–1260
76. Oisakede EO, Olawade DB, Bello OJ et al (2025) Cancer reversion therapy: prospects, progress and future directions. Curr Issues Mol Biol 47(12):1049
77. Zeppernick F, Meinhold-Heerlein I (2014) The new FIGO staging system for ovarian, fallopian tube, and primary peritoneal cancer. Arch Gynecol Obstet 290(5):839–842
78. Berek JS, Renz M, Kehoe S et al (2021) Cancer of the ovary, fallopian tube, and peritoneum: 2021 update. Int J Gynaecol Obstet 155(Suppl 1):61–85

79. Wang J, Gao J, Yao H et al (2014) Diagnostic accuracy of serum HE4, CA125 and ROMA in patients with ovarian cancer: a meta-analysis. Tumour Biol 35(6):6127–6138
80. Luo HJ, Hu ZD, Cui M et al (2023) Diagnostic performance of CA125, HE4, ROMA, and CPH-I in identifying primary ovarian cancer. J Obstet Gynaecol Res 49(3):998–1006
81. Chandler JE, Subramanian H, Maneval CD et al (2013) High-speed spectral nanocytology for early cancer screening. J Biomed Opt 18(11):117002
82. Roy HK, Turzhitsky V, Wali R et al (2017) Spectral biomarkers for chemoprevention of colonic neoplasia: a placebo-controlled double-blinded trial with aspirin. Gut 66(2):285–292
83. Ugander M, Oki AJ, Hsu LY et al (2012) Extracellular volume imaging by magnetic resonance imaging provides insights into overt and sub-clinical myocardial pathology. Eur Heart J 33(10):1268–1278
84. Moon JC, Messroghli DR, Kellman P et al (2013) Myocardial T1 mapping and extracellular volume quantification: a Society for Cardiovascular Magnetic Resonance and CMR Working Group of the European Society of Cardiology consensus statement. J Cardiovasc Magn Reson 15(1):92
85. Lyu L, Liu XL, Rui MP et al (2020) Liver extracellular volume fraction values obtained with magnetic resonance imaging can quantitatively stage liver fibrosis: a validation study in monkeys with nonalcoholic steatohepatitis. Eur Radiol 30(10):5748–5757
86. Liu JY, Wang Q, Lu YT et al (2025) MRI-derived extracellular volume fraction as a prognostic biomarker for early recurrence after R0 resection of pancreatic ductal adenocarcinoma. Eur J Radiol Open 15:100711
87. Adams LC, Jurmeister P, Ralla B et al (2019) Assessment of the extracellular volume fraction for the grading of clear cell renal cell carcinoma: first results and histopathological findings. Eur Radiol 29(11):5832–5843
88. Wang W, Fan X, Yang J et al (2023) Preliminary MRI study of extracellular volume fraction for identification of lymphovascular space invasion of cervical cancer. J Magn Reson Imaging 57(2):587–597
89. Li S, Liu J, Guo R et al (2023) T1 mapping and extracellular volume fraction measurement to evaluate the poor-prognosis factors in patients with cervical squamous cell carcinoma. NMR Biomed 36(8):e4918
90. Masramon M, Mathew M, Singh S et al (2026) Validating the biological origin of in vivo fractional intracellular volume from VERDICT-MRI in the prostate. Eur Radiol Exp 10(1):123
91. Bailey C, Bourne RM, Siow B et al (2019) VERDICT MRI validation in fresh and fixed prostate specimens using patient-specific moulds for histological and MR alignment. NMR Biomed 32(5):e4073
92. Nocera G, Sanvito F, Yao J et al (2025) Independent histological validation of MR-derived radio-pathomic maps of tumor cell density using image-guided biopsies in human brain tumors. J Neurooncol 175(1):111–122

93. Rao Y, Gammon S, Zacharias NM et al (2020) Hyperpolarized [1-13C]pyruvate-to-[1-13C]lactate conversion is rate-limited by monocarboxylate transporter-1 in the plasma membrane. Proc Natl Acad Sci U S A 117(36):22378–22389
94. Brindle KM (2015) Imaging metabolism with hyperpolarized 13C-labeled cell substrates. J Am Chem Soc 137(20):6418–6427
95. Zaric O, Farr A, Minarikova L et al (2021) Tissue sodium concentration quantification at 7.0-T MRI as an early marker for chemotherapy response in breast cancer: a feasibility study. Radiology 299(1):63–72
96. Zöllner FG, Konstandin S, Lommen J et al (2016) Quantitative sodium MRI of kidney. NMR Biomed 29(2):197–205
97. Bonekamp D, Schelb P, Wiesenfarth M et al (2019) Histopathological to multiparametric MRI spatial mapping of extended systematic sextant and MR/TRUS-fusion-targeted biopsy of the prostate. Eur Radiol 29(4):1820–1830
98. Lindgren A, Anttila M, Rautiainen S et al (2017) Primary and metastatic ovarian cancer: characterization by 3.0T diffusion-weighted MRI. Eur Radiol 27(9):4002–4012
99. Davarpanah AH, Kambadakone A, Holalkere NS et al (2016) Diffusion MRI of uterine and ovarian masses: identifying the benign lesions. Abdom Radiol (NY) 41(12):2466–2475
100. van Nagell JR Jr, Burgess BT, Miller RW et al (2018) Survival of women with type I and II epithelial ovarian cancer detected by ultrasound screening. Obstet Gynecol 132(5):1091–1100

Figures

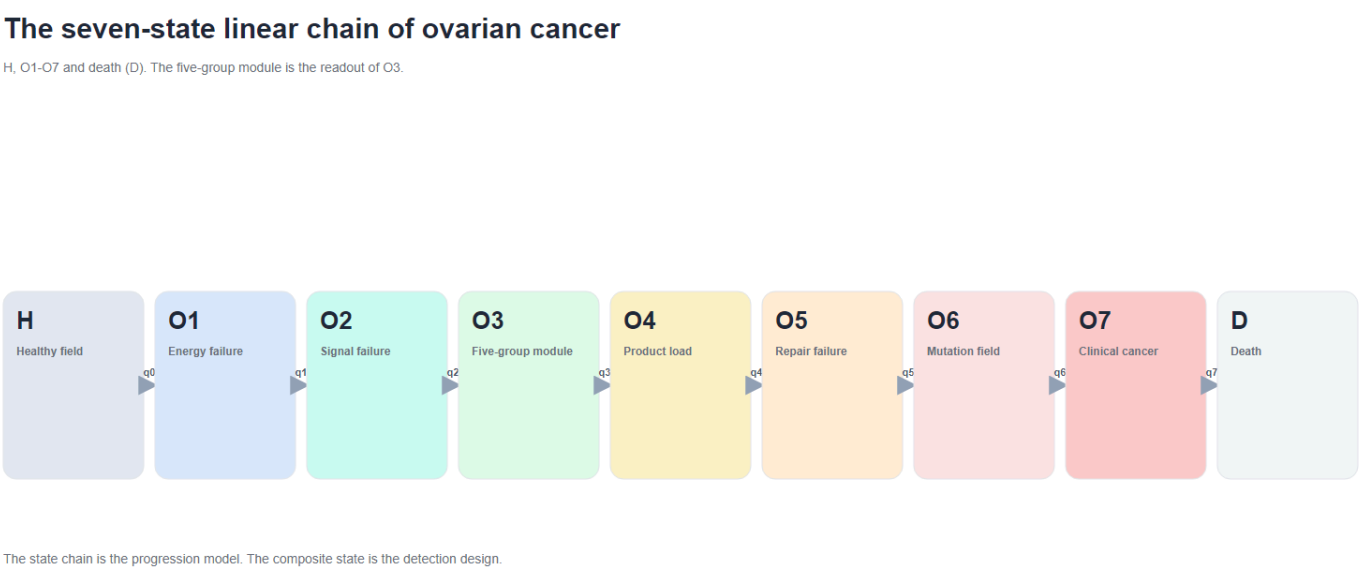


Figure 1

The seven-state linear chain of ovarian cancer. H, O1-O7 and death (D). The five-group module is the readout of O3; the six product groups are the readout of O4.

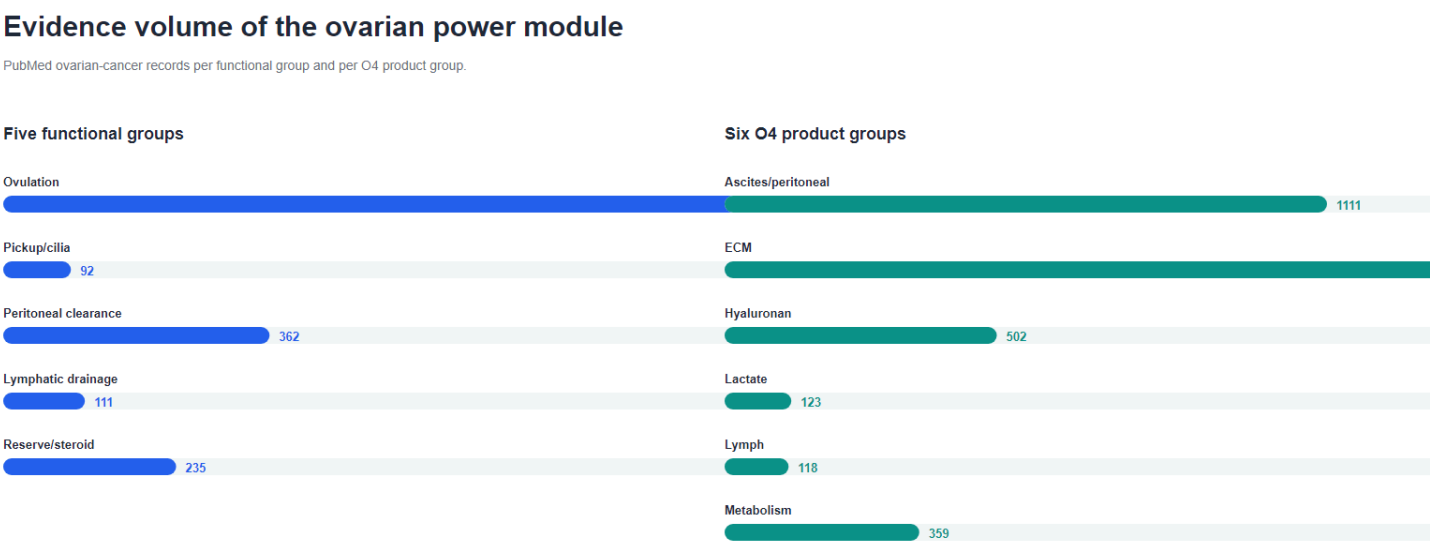


Figure 2

Evidence volume by group and product group. PubMed ovarian-cancer records for the five functional groups and the six O4 product groups.

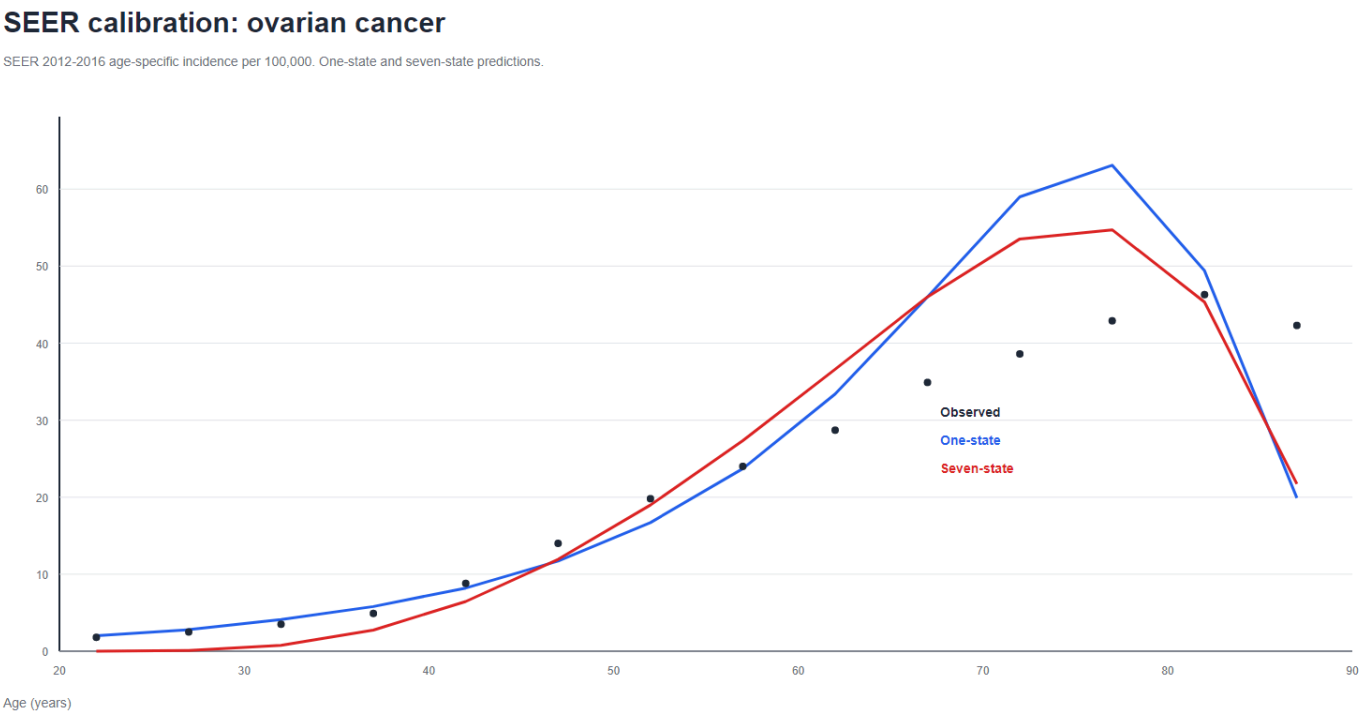


Figure 3

Calibration against SEER age-specific incidence. Observed and predicted age-specific incidence. The one-state model tracks the aggregate curve.

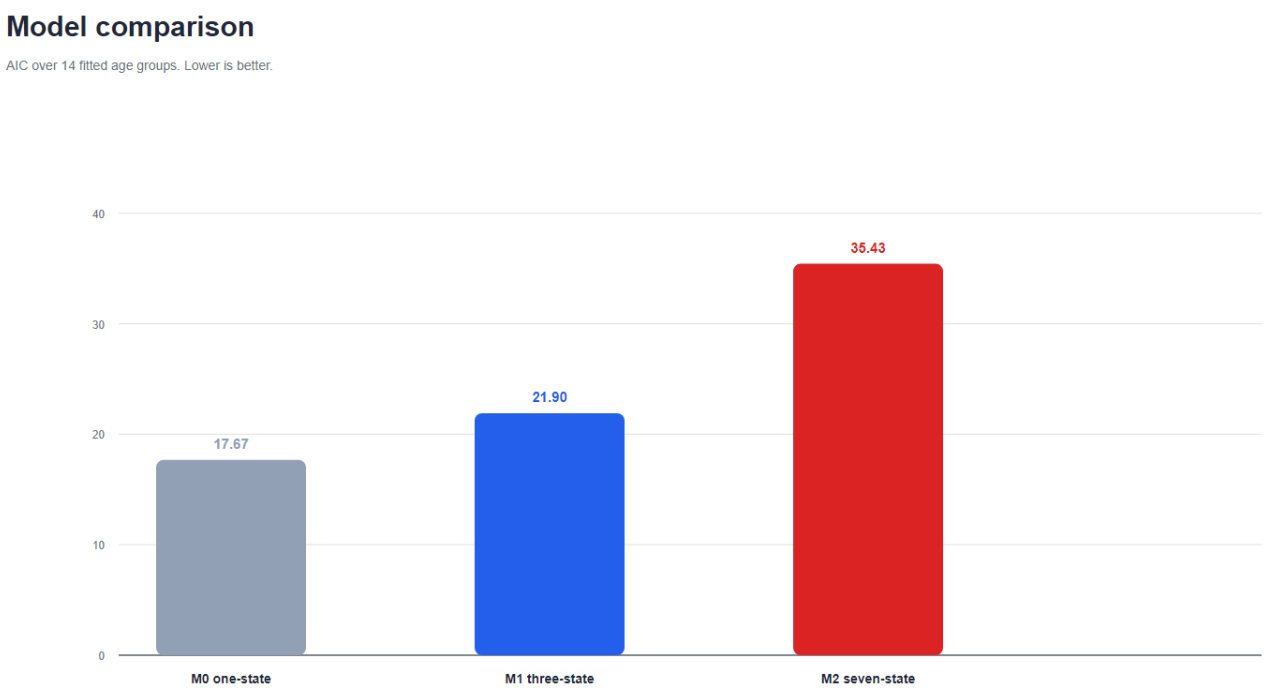


Figure 4

Model comparison. AIC and BIC for the one-state, three-state and seven-state models. The four intermediate rates collapse to one value.

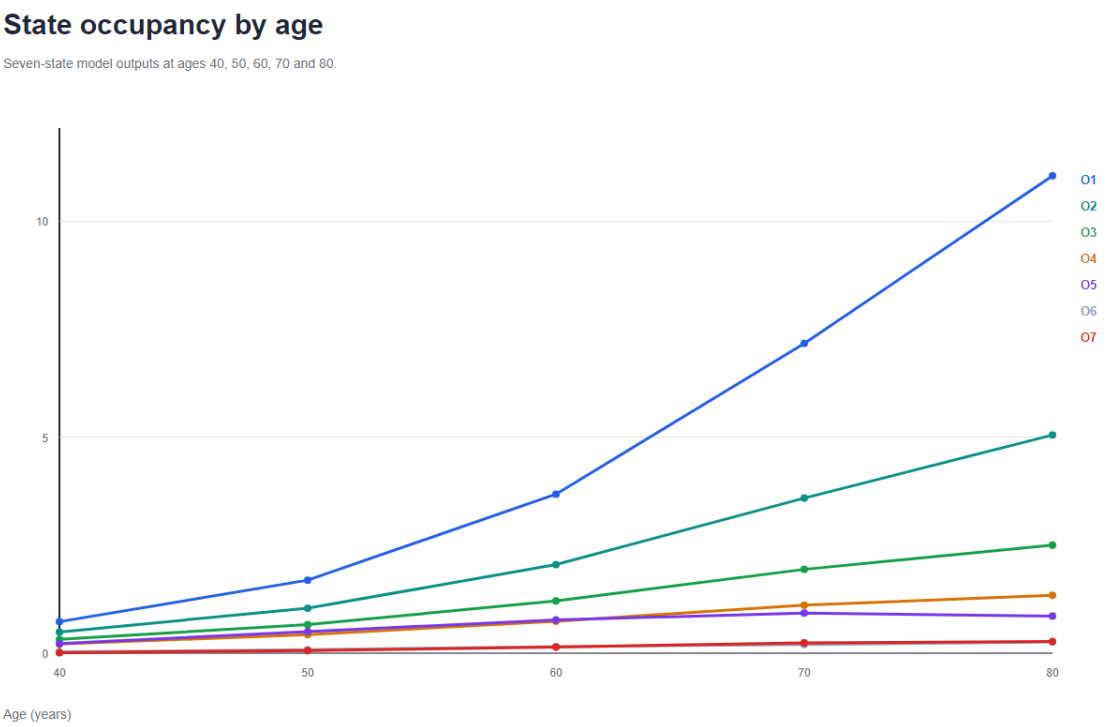


Figure 5

State occupancy by age. O1-O7 occupancy at ages 40, 50, 60, 70 and 80.

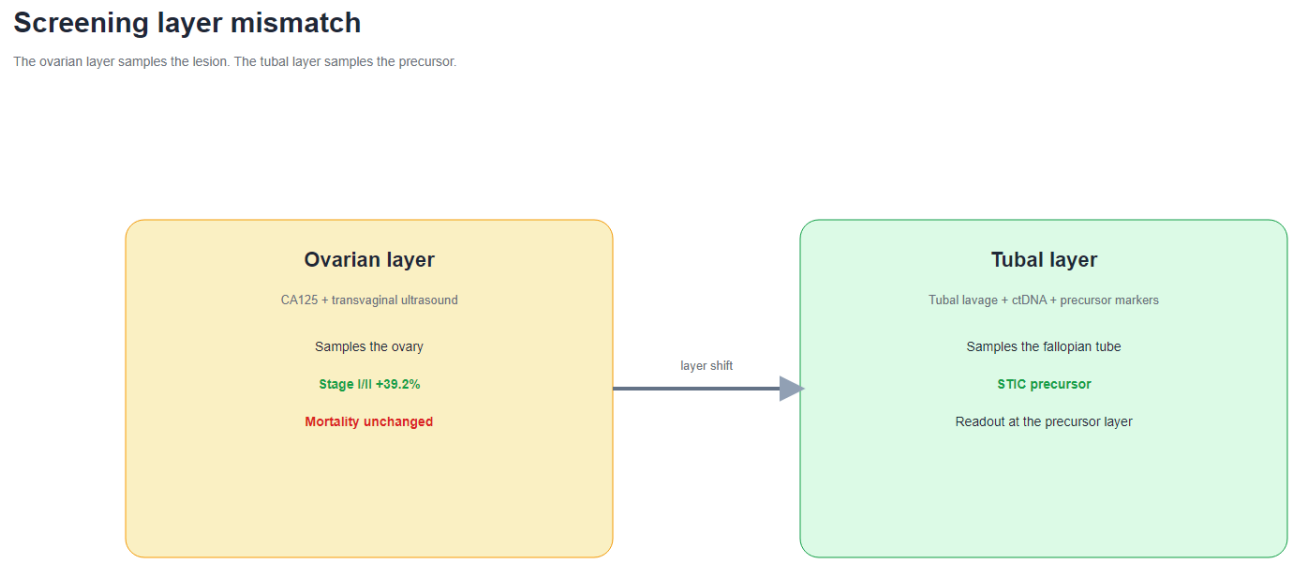


Figure 6

Screening layer mismatch. The ovarian layer samples the lesion. The tubal layer samples the precursor. UKCTOCS raised stage I/II detection by 39.2% and did not reduce mortality.

Supplementary Files

This is a list of supplementary files associated with this preprint. Click to download.

- SupplementaryTablesS1S7.docx